Photoemission during flash sintering: an interpretation based on thermal radiation

Mattia Biesuz[a, #], Piero Luchi[a], Alberto Quaranta[a], Alessandro Martucci[b], Vincenzo M. Sglavo[a]

[a] University of Trento, Department of Industrial Engineering
Via Sommarive 9
38123 Trento (TN) ITALY

[b] University of Padova, Department of Industrial Engineering
Via Marzolo 9
35131 Padova (PD) ITALY

[#] Corresponding author

e-mail: mattia.biesuz@unitn.it

Full text available at: https://www.sciencedirect.com/science/article/pii/S095522191730198X

Abstract

Optical emission spectra were recorded in the range 180-1700 nm during flash sintering of alumina and magnesia silicate glass-containing alumina. The collected spectra, corrected for taking care of instrumental effects, are consistent with thermal radiation effect. A partial exception is represented by the lower density samples treated with low current density, whose spectrum shows very small deviation from the expected thermal radiation at ~ 680 nm although the corresponding physical phenomenon remains unclear. In any case, the overall photoemission upon flash sintering can be substantially associated with Joule heating, in all tested conditions, with no effect of any other previously reported mechanism like electroluminescence.

Keywords: flash sintering; photoemission; alumina; glass-containing alumina; black body radiation

1 Introduction

The reduction of fossil fuels consumption and CO_2 emission is one of the main concerns for the research activity of the present century. Many projects are therefore focused on the development of green and environmental-friendly processing technologies. In particular, in the ceramics field, electrical field assisted sintering techniques have been recently proposed, they allowing significant reduction of sintering time and temperature. Among them, particular interest has been risen in the last few years by Flash Sintering (FS), such powder consolidation technology enabling to reduce the temperature needed for densification by several hundred degrees with respect to conventional processes [1,2]. In addition, densification occurs in just few seconds [2] while typical sintering usually requires some hours. Another important issue regards the possibility of using flash sintering on

materials with very different electrical behavior, from semiconductors [3] to insulators [4–6] or protonic [7,8], ionic [1,2,9–14] and electronic conductors[15,16]or even to composites[17].

For these reasons, the scientific interest on FS has rapidly increased and a certain number of works starts to try understanding the physical bases of the process. Recently, Todd[18], Zhang [19] and co-workers proposed a model for explaining the incubation of FS as a result of thermal runaway. Nevertheless, such works do not explain which mechanism is leading to densification [18]. As for this point, different hypotheses have been advanced, involving Joule heating [11], formation of Frenkel pairs [4], local overheating at the grain boundaries [4] or interaction between electrical field and space charge region [4].

Usually, FS phenomenon can be divided into three main stages. The first is the process incubation, during which the system works under voltage control and the current slowly increases. The second stage is characterized by an abrupt drop in material resistivity and the current density increases in an uncontrolled way. At this point a power peak is reached and the system is typically turned from voltage to current control in order to avoid the damage of the electric set-up and of the sample. The reasons behind such uncontrolled electrical conductivity increase are not completely clear, yet. Some works in the scientific literature show a good agreement between the measured conductivity and the conductivity evolution expected from temperature/density measurement [11]; other authors pointed out that during the flash the conduction can not be explained by the typical mechanisms associated with the electrical properties of materials[5,20,21]. The third and final FS stage (also known as steady stage) starts when the electric field is stabilized. During such stage the applied current is equal to the current limit of the system. The material densification occurs during the second and the third stage of the process. Densification and resistivity decrease are accompanied by other peculiar phenomena and, in particular, by bright emission of visible light [22–24]. The concomitant presence of these three phenomena allows to define the flash sintering process. Therefore, light emission represents an intrinsic footprint of FS.

Photoemission has always appeared quite unusual and interesting, and it has been studied in order to achieve further indications about the mechanisms involved during the whole process and, especially, on those promoting densification. Emission spectra have been recorded on YSZ by Lebrun [22] and Terauds et al. [23] in the visible and IR range. Also Naik et al. have performed similar measurements during potassium niobate and strontium titanate FS experiments [24], reporting a correlation between light emission intensity and sintering rates. All these authors concluded that the measured spectra show features far different from the black body radiation and explained the observed photoemission in terms of electroluminescence, as a result of the recombination between electrons and holes in the ceramic lattice [22]. Such phenomenona were tentatively attributed to a secondary effect of Frenkel pairs nucleation during the flash process[23]: it was suggested that vacancies and interstitials ionize in neutral defects promoting the formation of free electrons and holes, whose recombination causes electroluminescence. In the meantime, uncharged vacancy/interstitial pairs move under the effect of sintering potential, this generating rapid densification[25].

In 2015, McLaren et al. reproduced the flash event in bulk alkali silicate glasses. In such materials the flash event is associated to an unexpected drop in glass viscosity and, for this reason, it was named Electric Field Induced Softening (EFIS)[26]. Also in this case a strong bright light emission takes place during the process although it shows effects partially different with respect to crystalline ceramics.

Such differences are mainly associated to the fact that photoemission in glasses is characterized by very sharp peaks in the visible region. Yu et al., in a recent review on FS, argued that such peaks could be related to the oxidation-ionization of alkali metals (Li and Na), which causes photoemission peaks [27].

In the present work, we analyze the flash sintering behavior of two very common ceramics: nearly pure α-alumina and magnesia silicate glass-containing alumina. Such materials have already been successfully densified by FS and corresponding structural evolution has been deeply analyzed as a function of the main process parameters [5,6,28]. Here, we study the photoemission phenomena during FS in the UV/visible and NIR range with the aim to understand the mechanisms responsible for the observed optical phenomena further. The two materials were chosen in order to point out possible luminescent effects occurring in fully crystalline material and in glass-containing ceramic.

2 Experimental Procedures

α-alumina (Almatis CT3000SG) and magnesia silicate glass were used to produce dog bone-like samples by uniaxial pressing (maximum pressure = 120 MPa), using distilled water as binder (~ 5 wt%). The glass was obtained from TEOS and magnesium nitrate as precursor of silica and magnesia, respectively (as described in Ref. [28]). The nominal composition of the glass-containing alumina samples was 90 wt% alumina, 8 wt% silica and 2 wt% magnesia and they were obtained mixing α-alumina and glass (10 wt%) in isopropanol before uniaxial pressing. The gage section of the dog bone samples was 3 mm x 2.5 ± 0.3 mm. Other details regarding the samples geometry are reported in a previous work[29].

Pure alumina green specimens were pre-sintered for 2 h in a muffle furnace (Nabertherm) under static air atmosphere at 1250 and 1450°C. Glass-containing samples were pre-sintered at 950°C for 15 min. Heating rate of 10°C/min and free cooling within the furnace were used in both cases.

The relative density was measured by the Archimedes' method, using an analytical balance (Gibertini, sensitivity ± 0.0001 g). The grain size of pre-sintered sample was determined as an average of 12 measurements, which were carried out on SEM (JEOL, JSM 5500) micrographs using the linear intercept method [30].

After pre-sintering, the specimens were connected to a DC power supply (Glassman, 5 kV-120 mA) and to a multimeter (Keithley, 2100) by two platinum wires, which were forced within the holes realized on the opposite sides of the dog-bone sample. The samples were hung within a tubular furnace (Nabertherm P330) kept at constant temperature of 1200°C. The temperature was also continuously checked by an S-thermocouple placed close to the sample to guarantee that it was always between 1195 and 1205°C. Seven minutes after the sample was placed into the furnace, the power supply was switched on to promote the flash sintering of the specimen. For this purpose an electrical field (E-field) in the range 750-1000 V/cm was applied and the current limit was fixed at 4 mA/mm^2. Some specimens were also treated with different current limit (2 and 6 mA/mm^2) for comparison.

The optical emission during FS in the UV/VIS region was measured using the spectrometer USB4000 and the software "Ocean Optic Spectra Suite". The spectrometer was connected to a silica optical fiber, placed near the furnace tube in front of the sample. The background emission of the system

(furnace + sample at 1200°C) was initially recorded and subtracted from the spectra. Some spectra were also collected after the power supply was switched off to analyze the optical emission fading. The integration time was set to 3.8 ms and the mean of 5 collected successive spectra was considered. The optical response of the overall system as a function of wavelength was properly corrected: the spectrum generated by a calibration lamp (Avantes, HD2000) was recorded and the conversion factor was calculated as the ratio between the real emission from the lamp and the light yield measured from the spectrometer. This allowed therefore to calculate the real photoemission as the product of the conversion factor and the measured intensity at each wavelength.

Similar experimental set up and procedures were used for the measurement of photoemission in the NIR. In this case, an Ocean Optics NIR 512 spectrometer was used and the integration time was set to 10 ms. No spectral correction was performed for this spectrometer.

3 Results and Discussion

The bulk density of alumina samples pre-sintered at 1250°C is 2.73 g/cm^3 (relative density = 69%). The estimated average grain size is 0.37 μm. Samples treated at 1450°C exhibit density of 3.71 g/cm^3 (relative density = 94%) and grain size equal to 0.49 μm. Glass-containing alumina specimens are characterized by bulk density of 1.81 g/cm^3 after the pre-sintering treatment at 950°C.

The as-recorded optical emission spectra collected in the visible range during the third stage of FS on pure alumina samples pre-sintered at 1250°C are shown in Fig. 1. The light yield increases with the current limit, although the shape of the spectrum does not change. Quite surprisingly, the spectra obtained here very well compare with those shown in previous works on completely different materials, like YSZ and titanate/niobate, using similar experimental set up [22,24]. In particular, a shoulder around 620 nm and two maxima around 720 and 760 nm appear in all spectra. This first result seems to indicate that the emission in the 180-880 nm range does not depend upon the tested material and its composition.

The conversion factor, used for the calibration, is reported in Fig. 2. After the calibration, the shape of the spectra drastically changes, as shown in Fig. 3(a). The real emission intensity increases monothonically with the wavelength and only three small features can be identified in the spectra.

The first one is a slightly broad effect around 760 nm, which cannot be associated with specific electronic transition in corundum [31–39] and it is very likely related to some residual instrumental effect. As a matter of fact, the correction factor curve used for calibration shows the same peak in such region, as shown in Fig.2.

An inflection point can be detected at about 680 nm especially in the emission spectra collected using current densities of 2 and 4 A/mm^2. This is confirmed by the emission intensity derivative plot reported in the inset of Fig. 3(a) where a relative maximum can be identified at ~ 680 nm. Unfortunately, it is not easy to identify the reason also of such feature, the luminescence effects from alumina point defects, like F, F^+, or F_2 centers, being detected typically at lower wavelengths [33–39]. The inflection point disappears quite completely at 6 A/mm^2 and this could suggest a certain correlation between the observed effect and the presence of surfaces, the material becoming denser by increasing the applied current [5,28]. In addition, close to sharp pores, that are still present in samples sintered using with 2-4 mA/mm^2, [5,6] field and current are significantly

intensified [40,41]. Therefore, local effects that are not visible when higher currents are applied (dense material), may be activated at 2-4 mA/mm^2.

Finally, a small peak at 591 nm can be identified (inset in Fig. 1). This is probably related to the ionization of air near the electrodes. As a matter of fact, the intensity of such peak increases when sparkling occurs, while the peak disappears if the electrodes are shielded; in such case, no evidence of air ionization can be observed in any other part of the sample. It is also interesting to observe that the peak position could be associated to an emission line for ionized nitrogen [42].

Similar spectra were also recorded on magnesia silicate glass-containing alumina, as reported in Fig. 3(b). No specific peaks are detected also in such spectra, revealing slightly different results with respect to findings reported by McLaren et al. on alkali-containing glasses during electric field-induced softening[26].

The fundamental outcome of the performed optical analysis is that all spectra collected and calibrated in the present work resemble the black body emission spectrum. To make this point clearer we calculated the actual sample temperature (T_S) reached during the steady stage of FS as [2,5,20,43]:

$$T_S = \left(T_F^4 + \frac{E\,J\,V}{S\,\sigma\,\varepsilon}\right)^{0.25} \qquad (1)$$

where T_F is the furnace temperature, σ the Stefan constant, E the electric field, J the current density, S, V and ε the specimen surface, volume and emissivity[5,28], respectively. Then, Black Body Spectra (BBS), as calculated by the Planck's law[44] at different sample temperature, were plotted in Fig. 3, with the aim to provide a qualitative comparison with the measured spectral shape. Although some deviation can be observed, the sample photoemission is characterized by a good affinity with BBS.

As shown in Figures 3, the light yield increases with the current density, this being very likely correlated to the Joule heating of the material. The equilibrium temperature in the specimen increases, according to Eq. 1, with the current limit. As a consequence, it is not surprising that the samples treated with 6 mA/mm^2 are hotter and brighter than those treated with lower currents.

A more detailed analysis of the light emission evolution during the process was carried out for pure alumina sample pre-sintered at 1450°C and treated with 750 V/cm - 4 mA/mm^2 the obtained results being representative of those recorded also on the other materials. Figure 4 shows the correlation between photoemission intensity and electrical parameters of the system, i.e. voltage, current and power dissipation. One can observe that the shape of the spectrum does not change during the runaway while the emission intensity increases. The shape well resembles typical thermal emission diagrams, this confirming that the observed visible light emission is mainly due to thermal processes upon the three FS stages. As shown in Fig. 4, after the system reaches the current limit, the emission intensity keeps on increasing (between 600 s and 605 s) for several seconds because the sample surface temperature does. This time lag is needed for balancing the electrical power generated in the sample and the radiative heat release. Once the sample temperature is stabilized, photoemission, applied voltage and power dissipation become simultaneously substantially constant. These results suggest that the highest temperature during FS is not reached at the power peak (when the system switches from voltage to current control) but during the steady stage of the process. It is worth noting that the voltage drop from the power peak and the steady stage (Fig. 4(a))

can not be associated to microstructural evolution due to sintering, the tested sample being pre-sintered at 1450° (relative density = 94%). Therefore, the observed electrical behavior points out an increase of sample temperature after the power peak, consistent with the increased light yield.

No inflection point can be identified at 680 nm in such spectra, this pointing out that the intrinsic optical emission is lower than the detection limit of the measuring apparatus. This result can be related to the more compact structure of samples pre-sintered at 1450 °C characterized by larger density and grain size.

The light yield decay for alumina sample was measured after switching the power supply off, in order to point out other affinities between thermal radiation and photoemission. The results are summarized in Fig. 5. One can observe that light emission takes several seconds to be reduced, the decay process being quite slow. This behavior is not coherent with luminescent phenomena, which should decay within few microseconds at the longest. Conversely, the reported behavior can be again explained in terms of thermal radiation, the temperature requiring several seconds to reach the equilibrium.

In a previous work, Terauds et al. [23] observed two emission peaks in the NIR, at about 1175 and 2250 nm, during flash sintering of YSZ. In order to verify the presence of similar features in alumina and glass-containing alumina, we carefully analyzed light emission in the region between 900 and 1700 nm. The spectra collected during the third stage of flash sintering and at different current limits, normalized with respect to the maximum light intensity, are reported in Fig. 6. Once again, the shape of the light emission spectrum does not change with the applied current. Interestingly, very similar plots are obtained also from the light emitted by the empty hot furnace alumina tube used in the present work, this confirming that also in the NIR region the light emission upon FS is compatible with thermal radiation, only. The main, although limited, difference consists in a moderate light yield increase at low wavelength when the current density increases, this result being coherent with a blue shift of the thermal radiation at high currents and temperatures

Figure 7 shows the integrated light emission in the NIR range as a function of the electrical power dissipated during the third stage of flash sintering. One can observe that the light yield increases with the electrical power, following a nearly linear relation. This is again coherent with a thermal radiation phenomenon. In fact, during the third stage of flash sintering an equilibrium between electrical and radiative power is reached. One can consider that the sample temperature increases with power dissipation and the thermal emission maximum shifts to lower wavelength, moving closer or within the detection interval; this effect can explain the observed deviation from linearity in Fig. 7. Consequently, it should be not surprising that the light yield is overestimated or underestimated in the case of limited or large power dissipation, respectively.

Finally, an additional consideration can be advanced on the basis of the obtained results. In some previous works, the field-induced formation of Frenkel pairs has been claimed for explaining the densification behavior during FS [4]. No relevant signals can be detected in Fig. 1 at 188 nm and 255 nm, which can be associated to the annihilation of the Frenkel pairs for aluminum and oxygen, respectively, the formation energy of such defects in corundum being 4.87 and 6.59 eV [32]. The results obtained here do not match with the formation of Frenkel pairs upon flash sintering. Nevertheless, it is important to remind that the recombination of defects can also produce a non-radiative decay through the emission of heat in form of phonons.

4 Conclusions

A careful analysis of the optical spectra recorded in the visible/near infrared range upon flash sintering of alumina and magnesia silicate glass-containing alumina points out that the main contribution to radiation emission is of thermal origin. Only some very small features in the photoemission spectra at about 591 nm and ~ 680 nm, whose origin remains unclear, could be related to athermal effects. In any case, light emission during flash sintering can not attributed to electroluminescent phenomena or to intrinsic luminescent centers of the lattice.

References

[1] J.A. Downs, V.M. Sglavo, Electric field assisted sintering of cubic zirconia at 390°C, J. Am. Ceram. Soc. 96 (2013) 1342–1344.

[2] M. Cologna, B. Rashkova, R. Raj, Flash sintering of nanograin zirconia in <5 s at 850°C, J. Am. Ceram. Soc. 93 (2010) 3556–3559.

[3] E. Zapata-Solvas, S. Bonilla, P.R. Wilshaw, R.I. Todd, Preliminary investigation of flash sintering of SiC, J. Eur. Ceram. Soc. 33 (2013) 2811–2816.

[4] M. Cologna, J.S.C. Francis, R. Raj, Field assisted and flash sintering of alumina and its relationship to conductivity and MgO-doping, J. Eur. Ceram. Soc. 31 (2011) 2827–2837.

[5] M. Biesuz, V.M. Sglavo, Flash sintering of alumina: Effect of different operating conditions on densification, J. Eur. Ceram. Soc. 36 (2016) 2535–2542.

[6] M. Biesuz, V.M. Sglavo, Flash sintering of alumina and its microstructural evolution, Ceram. Eng. Sci. Proc. 37 (2016).

[7] R. Muccillo, E.N.S. Muccillo, M. Kleitz, Densification and enhancement of the grain boundary conductivity of gadolinium-doped barium cerate by ultra fast flash grain welding, J. Eur. Ceram. Soc. 32 (2012) 2311–2316.

[8] T. Jiang, Y. Liu, Z. Wang, W. Sun, J. Qiao, K. Sun, An improved direct current sintering technique for proton conductor - BaZr0.1Ce0.7Y0.1Yb0.1O3: The effect of direct current on sintering process, J. Power Sources. 248 (2014) 70–76.

[9] R. Muccillo, M. Kleitz, E.N.S. Muccillo, Flash grain welding in yttria stabilized zirconia, J. Eur. Ceram. Soc. 31 (2011) 1517–1521.

[10] R. Baraki, S. Schwarz, O. Guillon, Effect of electrical field/current on sintering of fully stabilized zirconia, J. Am. Ceram. Soc. 95 (2012) 75–78.

[11] Y. Du, A.J. Stevenson, D. Vernat, M. Diaz, D. Marinha, Estimating Joule heating and ionic conductivity during flash sintering of 8YSZ, J. Eur. Ceram. Soc. 36 (2016) 749–759.

[12] X. Hao, Y. Liu, Z. Wang, J. Qiao, K. Sun, A novel sintering method to obtain fully dense gadolinia doped ceria by applying a direct current, J. Power Sources. 210 (2012) 86–91.

[13] T. Jiang, Z. Wang, J. Zhang, X. Hao, D. Rooney, Y. Liu, W. Sun, J. Qiao, K. Sun, Understanding the flash sintering of rare-earth-doped ceria for solid oxide fuel cell, J. Am. Ceram. Soc. 98

(2015) 1717–1723.

[14] M. Biesuz, G. Dell'Agli, L. Spiridigliozzi, C. Ferone, V.M. Sglavo, Conventional and field-assisted sintering of nanosized Gd-doped ceria synthesized by co-precipitation, Ceram. Int. 42 (2016) 11766–11771.

[15] A.L.G. Prette, M. Cologna, V. Sglavo, R. Raj, Flash-sintering of Co2MnO4 spinel for solid oxide fuel cell applications, J. Power Sources. 196 (2011) 2061–2065.

[16] A. Gaur, V.M. Sglavo, Densification of La0.6Sr0.4Co0.2Fe0.8O3 ceramic by flash sintering at temperature less than 100 °C, J. Mater. Sci. 49 (2014) 6321–6332.

[17] K.S. Naik, V.M. Sglavo, R. Raj, Field assisted sintering of ceramic constituted by alumina and yttria stabilized zirconia, J. Eur. Ceram. Soc. 34 (2014) 2435–2442.

[18] R.I. Todd, E. Zapata-Solvas, R.S. Bonilla, T. Sneddon, P.R. Wilshaw, Electrical characteristics of flash sintering: Thermal runaway of Joule heating, J. Eur. Ceram. Soc. 35 (2015) 1865–1877.

[19] Y. Zhang, J. Il Jung, J. Luo, Thermal runaway, flash sintering and asymmetrical microstructural development of ZnO and ZnO-Bi2O3 under direct currents, Acta Mater. 94 (2015) 87-100.

[20] R. Raj, Joule heating during flash-sintering, J. Eur. Ceram. Soc. 32 (2012) 2293–2301.

[21] S.K. Jha, R. Raj, The effect of electric field on sintering and electrical conductivity of Titania, J. Am. Ceram. Soc. 97 (2014) 527–534.

[22] J.M. Lebrun, R. Raj, A first report of photoemission in experiments related to flash sintering, J. Am. Ceram. Soc. 97 (2014) 2427–2430.

[23] K. Terauds, J.M. Lebrun, H.H. Lee, T.Y. Jeon, S.H. Lee, J.H. Je, R. Raj, Electroluminescence and the measurement of temperature during Stage III of flash sintering experiments, J. Eur. Ceram. Soc. 35 (2015) 3195–3199.

[24] K. Naik, S.K. Jha, R. Raj, Correlations between conductivity, electroluminescence and flash sintering, Scr. Mater. 118 (2016) 1–4.

[25] R. Raj, M. Cologna, J.S.C. Francis, Influence of externally imposed and internally generated electrical fields on grain growth, diffusional creep, sintering and related phenomena in ceramics, J. Am. Ceram. Soc. 94 (2011) 1941–1965.

[26] C. McLaren, W. Heffner, R. Tessarollo, R. Raj, H. Jain, Electric field-induced softening of alkali silicate glasses, Appl. Phys. Lett. 107 (2015) 184101.

[27] M. Yu, S. Grasso, R. Mckinnon, T. Saunders, M. Reece, Review of flash sintering : Materials , Mechanisms and Modelling, Adv. Appl. Ceram. Struct. , Funct. Bioceram. 116 (2017) 24–60.

[28] M. Biesuz, V.M. Sglavo, Liquid phase flash sintering in magnesia silicate glass-containing alumina, J. Eur. Ceram. Soc. 37 (2017) 705–713.

[29] J. Downs, Mechanisms of Flash Sintering in Cubic Zirconia, University of Trento, 2013. http://eprints-phd.biblio.unitn.it/976/.

[30] R.E. Chinn, Ceramography, ASM International, USA, 2002.

[31] M. Gaft, R. Reisfeld, G. Panczer, Modern Luminescence Spectroscopy of Minerals and Materials, II, Springer Mineralogy, 2015.

[32] K.P.D. Lagerlof, R.W. Grimes, The Defect Chemistry of Sapphire, Acta Mater. 46 (1998) 5689–5700.

[33] E.C. Kouroukla, I.K. Bailiff, I. Terry, L. Bowen, Luminescence characterisation of alumina substrates using cathodoluminescence microscopy and spectroscopy, Radiat. Meas. 71 (2014) 117–121.

[34] B.D. Evans, M. Stapelbroek, Optical properties of the F+ center in crystalline Al2O3, Phys. Rev. B. 18 (1978) 7089–7098.

[35] B.D. Evans, G.J. Pogatshnik, Y. Chen, Optical properties of lattice defects in a-Al2O3, Nucl. Inst. Methods Phys. Res. B. 91 (1994) 258–262.

[36] T. Sato, S. Kobayashi, S. Michizono, Y. Saito, Measurements of secondary electron-emission coefficients and cathodoluminescence spectra for annealed alumina ceramics, Appl. Surf. Sci. 144–145 (1999) 324–328.

[37] V.S. Kortov, A.E. Ermakov, A.F. Zatsepin, S. V. Nikiforov, Luminescence properties of nanostructured alumina ceramic, Radiat. Meas. 43 (2008) 341–344.

[38] J.H. Crawford, Defects and defect processes in ionic oxides: Where do we stand today?, Nucl. Inst. Methods Phys. Res. B. 1 (1984) 159–165.

[39] V.S. Kortov, V.A. Pustovarov, T. V. Shtang, Radiation-induced transformations of luminescence centers in anion-defective alumina crystals under high-dose irradiations, Nucl. Instruments Methods Phys. Res. Sect. B. 353 (2015) 42–45.

[40] T.B. Holland, U. Anselmi-Tamburini, D. V. Quach, T.B. Tran, A.K. Mukherjee, Local field strengths during early stage field assisted sintering (FAST) of dielectric materials, J. Eur. Ceram. Soc. 32 (2012) 3659–3666.

[41] M. Biesuz, P. Luchi, A. Quaranta, V.M. Sglavo, Theoretical and phenomenological analogies between flash sintering and dielectric breakdown in α-alumina, J. Appl. Phys. 120 (2016) 145107.

[42] S. Oss, L.M. Gratton, T. Lopez-Arias, Spark spectroscopy and the emission spectrum of air made easy, Phys. Educ. 426 (2013) 426–429.

[43] S. Grasso, Y. Sakka, N. Rendtorff, C. Hu, G. Maizza, H. Borodianska, O. Vasylkiv, Modeling of the temperature distribution of flash sintered zirconia, J. Ceram. Soc. Japan. 119 (2011) 144–146.

[44] J.H. Lienhard IV, J.H. Lienhard V, A heat transfer textbook, III, Phlogiston Press, 2008.

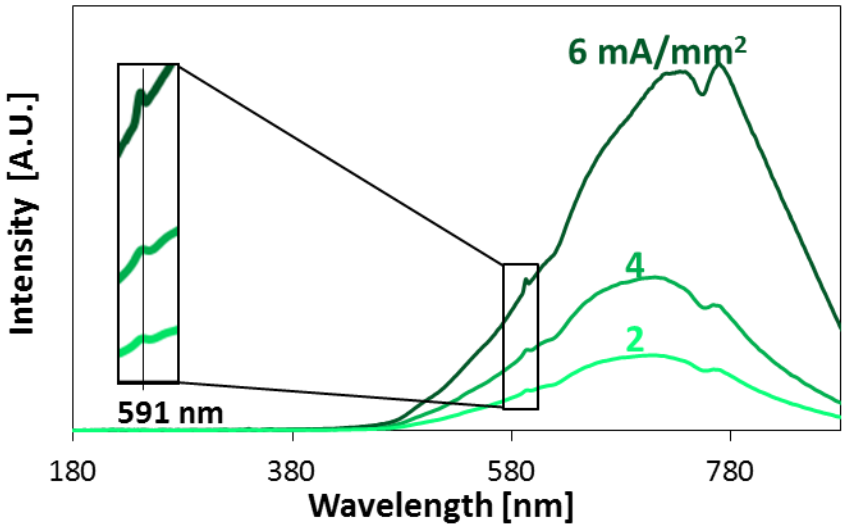

Figure 1: As collected optical emission spectra collected during the steady stage of flash sintering at different current density on pure alumina (pre-sintered at 1250°C; furnace temperature = 1200°C).

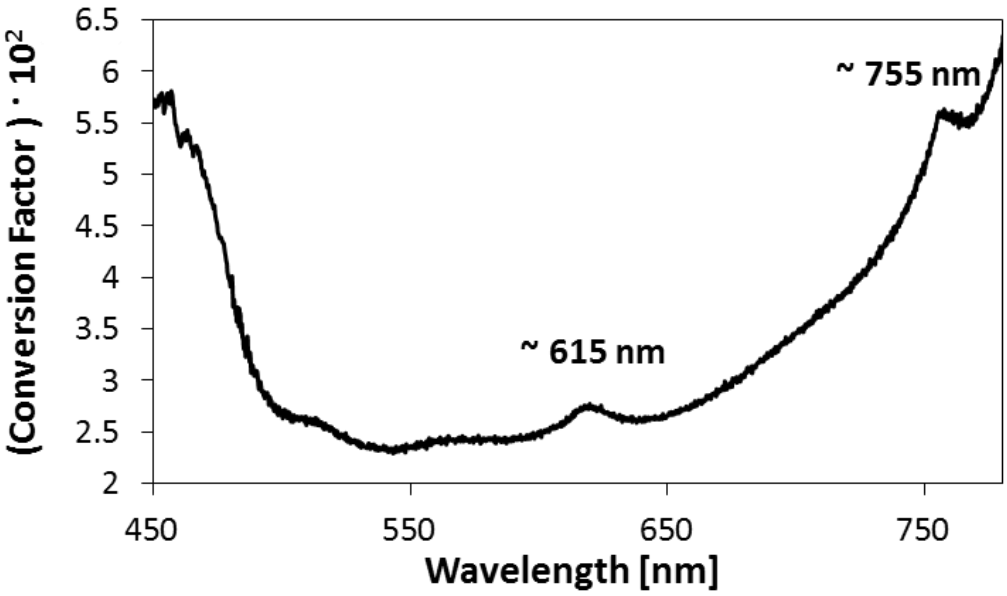

Figure 2: Conversion curve used for calibration.

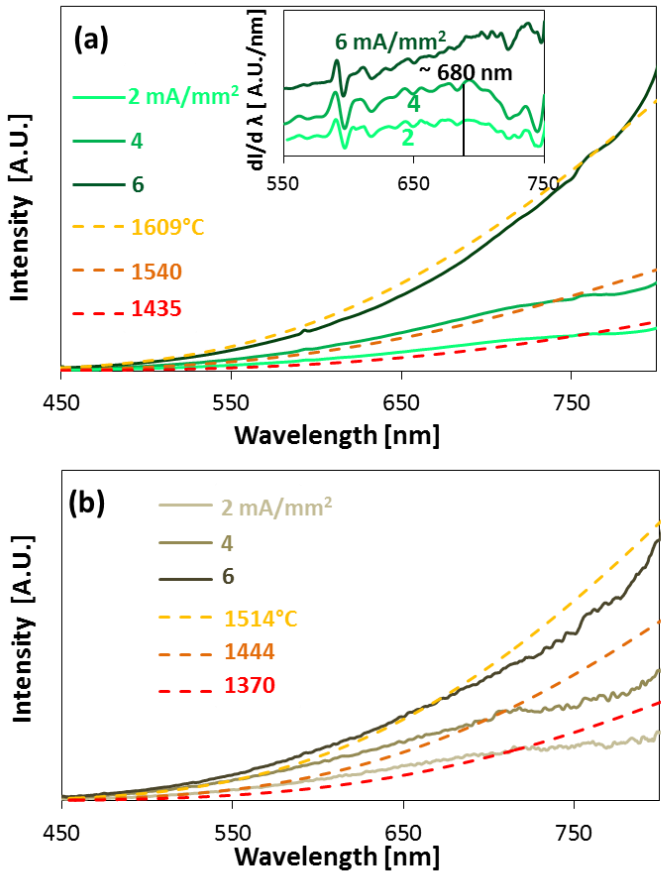

Figure 3: Calibrated optical emission spectra collected during the steady stage of flash sintering at different current density on pure alumina (pre-sintered at 1250°C; furnace temperature 1200°C) (a) and glass-containing alumina (b); black body spectra at the corresponding sample temperatures are reported for a qualitative comparison. The inset in (a) represents the derivative with respect to the wavelength of the emission intensity.

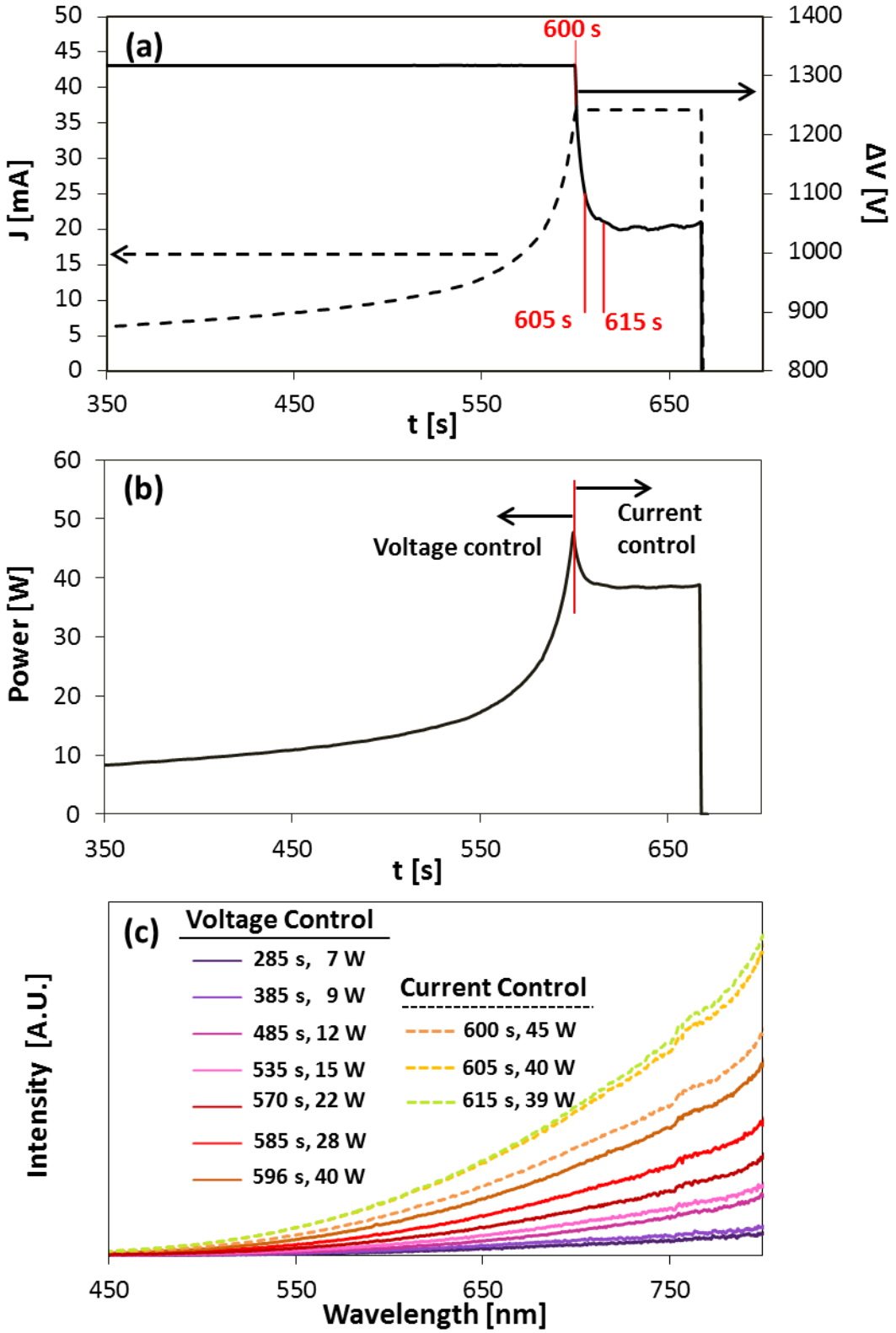

Figure 4: Current and voltage (a), power dissipation (b) and calibrated optical emission intensity (c) during the runaway for flash sintering of alumina (750 V/cm, 4 mA/mm^2, furnace temperature = 1200°C, pre-sintering at T = 1450°C). Time is zero when the power supply is turned on.

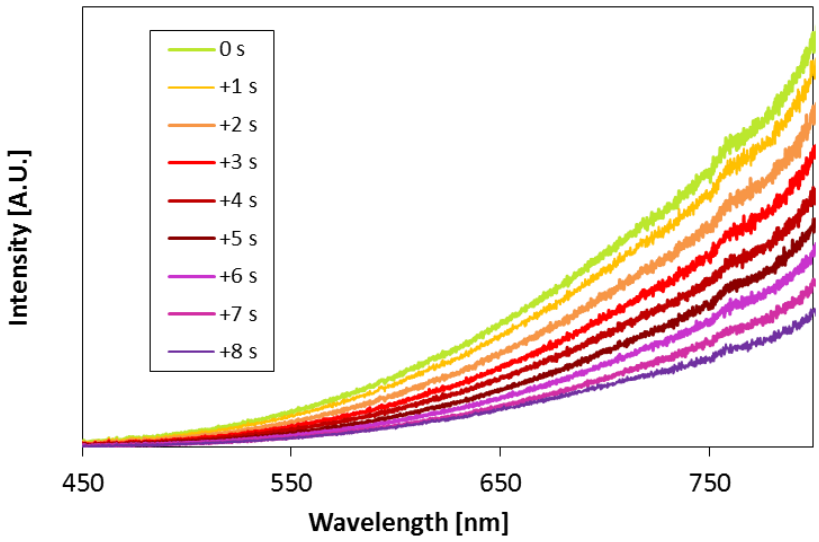

Figure 5: Optical emission decay after the power supply turn-off for alumina sample pre-sintered at 1450°C and treated with 4 mA/mm^2 (furnace temperature = 1200°C). The power supply was switched off between t = 0 s and t = 1 s.

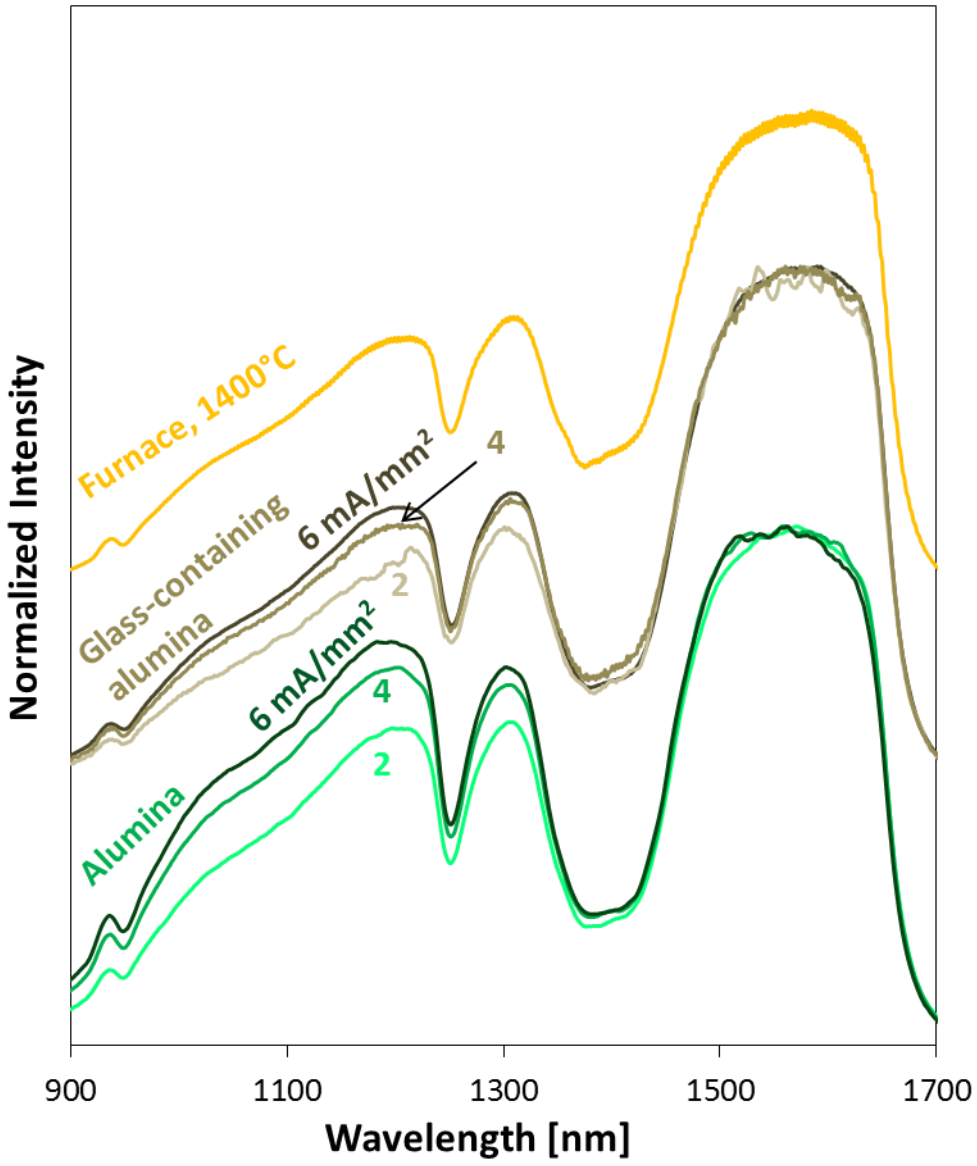

Figure 6: Normalized NIR optical emission during the third stage of flash sintering for pure alumina and glass-containing alumina (furnace temperature = 1200°C). The emission of the tubular furnace measured at 1400°C is reported for comparison.

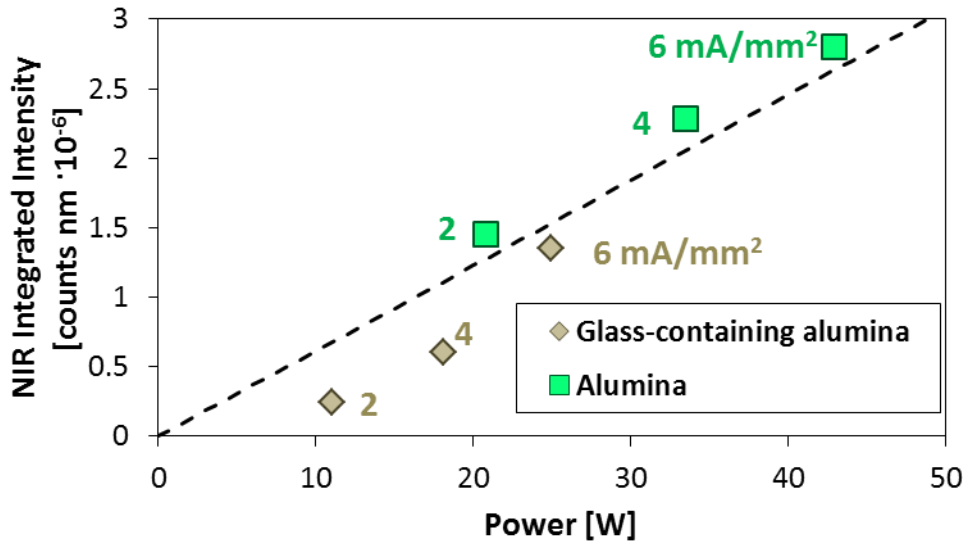

Figure 7: Integrated NIR optical emission intensity during the third stage of FS for pure alumina and glass-containing alumina as a function of the electrical power dissipation (furnace temperature = 1200°C).